





RESEARCH ARTICLE | APRIL 15 2024

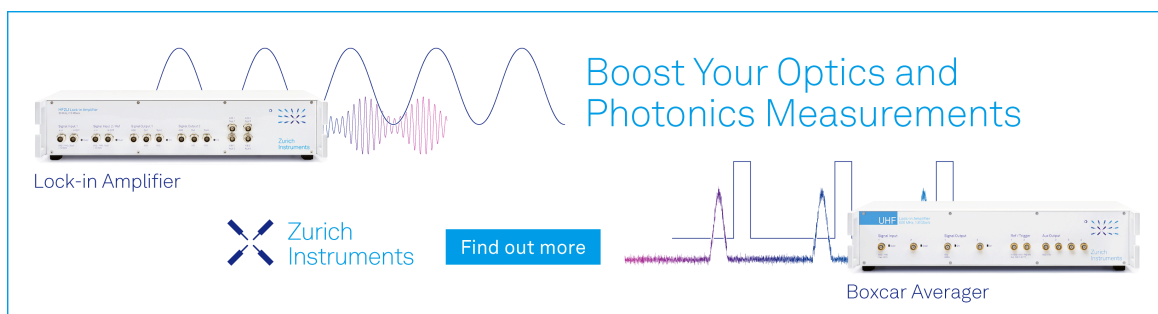
## The photochemistry of Rydberg-excited cyclobutanone: Photoinduced processes and ground state dynamics

J. Eng ; C. D. Rankine ; T. J. Penfold  




*J. Chem. Phys.* 160, 154301 (2024)

<https://doi.org/10.1063/5.0203597>



Boost Your Optics and Photonics Measurements

Lock-in Amplifier

 Zurich Instruments

[Find out more](#)

Boxcar Averager

# The photochemistry of Rydberg-excited cyclobutanone: Photoinduced processes and ground state dynamics

Cite as: J. Chem. Phys. 160, 154301 (2024); doi: 10.1063/5.0203597

Submitted: 15 February 2024 • Accepted: 28 March 2024 •

Published Online: 15 April 2024



View Online



Export Citation



CrossMark

J. Eng,<sup>1,a)</sup>  C. D. Rankine,<sup>2</sup>  and T. J. Penfold<sup>1,b)</sup> 

## AFFILIATIONS

<sup>1</sup>Chemistry, School of Natural and Environmental Sciences, Newcastle University, Newcastle Upon Tyne NE1 7RU, United Kingdom

<sup>2</sup>Department of Chemistry, University of York, York YO10 5DD, United Kingdom

**Note:** This paper is part of the JCP Special Topic on Prediction Challenge: Cyclobutanone Photochemistry.

<sup>a)</sup>Electronic mail: [julien.eng@newcastle.ac.uk](mailto:julien.eng@newcastle.ac.uk)

<sup>b)</sup>Author to whom correspondence should be addressed: [tom.penfold@newcastle.ac.uk](mailto:tom.penfold@newcastle.ac.uk)

## ABSTRACT

Owing to ring strain, cyclic ketones exhibit complex excited state dynamics with multiple competing photochemical channels active on the ultrafast timescale. While the excited state dynamics of cyclobutanone after  $\pi^* \leftarrow n$  excitation into the lowest-energy excited singlet ( $S_1$ ) state has been extensively studied, the dynamics following  $3s \leftarrow n$  excitation into the higher-lying singlet Rydberg ( $S_2$ ) state are less well understood. Herein, we employ fully quantum multiconfigurational time-dependent Hartree (MCTDH) simulations using a model Hamiltonian as well as “on-the-fly” trajectory-based surface-hopping dynamics (TSHD) simulations to study the relaxation dynamics of cyclobutanone following  $3s \leftarrow n$  excitation and to predict the ultrafast electron diffraction scattering signature of these relaxation dynamics. Our MCTDH and TSHD simulations indicate that relaxation from the initially-populated singlet Rydberg ( $S_2$ ) state occurs on the timescale of a few hundreds of femtoseconds to a picosecond, consistent with the symmetry-forbidden nature of the state-to-state transition involved. There is no obvious involvement of excited triplet states within the timeframe of our simulations (<2 ps). After non-radiative relaxation to the electronic ground state ( $S_0$ ), vibrationally hot cyclobutanone has sufficient internal energy to form multiple fragmented products including  $C_2H_4 + CH_2CO$  (C2; 20%) and  $C_3H_6 + CO$  (C3; 2.5%). We discuss the limitations of our MCTDH and TSHD simulations, how these may influence the excited state dynamics we observe, and—ultimately—the predictive power of the simulated experimental observable.

© 2024 Author(s). All article content, except where otherwise noted, is licensed under a Creative Commons Attribution (CC BY) license (<https://creativecommons.org/licenses/by/4.0/>). <https://doi.org/10.1063/5.0203597>

## I. INTRODUCTION

Ketones, i.e., organic compounds containing a carbonyl group, are among the simplest chromophores owing to their small size and low density of valence electronically excited states. Consequently, their photochemistry has been studied for several decades.<sup>1,2</sup> Cyclic ketones form an important subclass of these systems: Despite their apparently equivalent simplicity, their photochemistry is often comparatively complex and features activity across multiple competing photochemical channels most commonly characterized as Norrish Type I processes. In such a process, and upon excitation of an electron from the nonbonding orbital ( $n$ ) on the carbonyl oxygen atom

to the antibonding ( $\pi^*$ ) molecular orbital of the carbonyl group, a carbon–carbon bond adjacent to the carbonyl group (i.e.,  $C_\alpha$ ; Fig. 1) cleaves, opening up the possibility for formation of a variety of fragmentary products on the electronic ground state surface after non-radiative relaxation. As an exemplar cyclic ketone, cyclobutanone has particular photochemistry owing to the high degree of ring strain in the cyclobutane ring (arising as a consequence of the small ring size).<sup>3</sup> The particular photochemistry of cyclobutanone has attracted significant interest from both an experimental<sup>3–16</sup> and theoretical<sup>17–24</sup> perspective.

Many of these previous studies on cyclobutanone have aimed at elucidating the photochemistry and, in particular, the excited

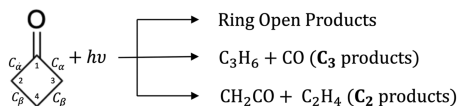


FIG. 1. Schematic of cyclobutanone and the potential photoproducts identified in previous work.

state dynamics arising from excitation at the weak  $S_1 \leftarrow S_0$  absorption band ( $\sim 330$ – $240$  nm) associated with the symmetry-forbidden  $\pi^* \leftarrow n$  transition. Early ultrafast spectroscopy of cyclobutanone in the gas phase carried out by the authors of the work of Diau *et al.*<sup>10</sup> revealed that, upon excitation at 307 nm (i.e., slightly above energy of the  $\pi^* \leftarrow n$  transition by  $\sim 2$  kcal mol<sup>-1</sup>)  $\alpha$ -cleavage occurs on a timescale of  $\sim 5$  ps, driven initially by the (i) cyclobutane ring puckering, (ii) carbonyl out-of-plane wagging, and (iii) carbonyl stretching modes. Following along the  $\alpha$ -cleavage channel, an  $S_1/S_0$  conical intersection (CI) is encountered via which non-radiative relaxation to the electronic ground state can proceed; this channel ultimately leads to the production of either (i) a vibrationally hot cyclobutanone on the  $S_0$  state, (ii) diradical intermediates that fragment to yield  $C_2H_4 + CH_2CO$  (C2 products), or (iii)  $C_3H_6 + CO$  (C3 products). The C3:C2 fragmentation quantum yields are known to exhibit a strong wavelength dependence;<sup>4,7,8,13,25</sup> the C3:C2 product ratio is reported to be 0.5 on excitation at 313 nm and to increase to 0.8 at 248 nm and 1.0 at 200 nm.<sup>13,26</sup> At wavelengths longer than 315 nm, there is a marked increase in the C3:C2 product ratio; it is reported to be 2.0 at 326 nm and as high as 7.0 at 344 nm.<sup>7,26</sup> The increase is indicative of an alternative dormant mechanism in the  $S_1$  state, which becomes operational at longer wavelengths; this alternative mechanism is proposed to involve photochemistry on the triplet manifold<sup>26</sup> as there is insufficient energy available at longer wavelengths to overcome the barrier encountered along the  $\alpha$ -cleavage channel and access the  $S_1/S_0$  CI. This mechanistic picture of cyclobutanone in the gas phase is largely maintained in solution as evidenced in the work of Kao *et al.*<sup>3</sup> Norrish Type I  $\alpha$ -cleavage is known to occur on the sub-picosecond timescale in solution. The involvement of photochemistry on the triplet manifold has been invoked in Norrish-type mechanisms,<sup>13</sup> and the authors of the work of Kao *et al.*<sup>3</sup> concede that—even with sufficient excess energy available to overcome the barrier encountered along the  $\alpha$ -cleavage channel—triplet states may still play a mechanistic role, although this is likely limited to indirect channels active on timescales longer than 500 ps.<sup>3</sup>

The second absorption band of cyclobutanone is located between  $\sim 206$  and 182 nm and is assigned to the  $3s \leftarrow n$  transition into the second electronically excited singlet state ( $S_2$ ): a state that exhibits Rydberg character.<sup>14</sup> The authors of the work of Trentelman *et al.*<sup>15</sup> have studied the 193 nm photolysis of cyclobutanone, reporting that 57% of the electronically excited state species form the C3 products, 30% form the C2 products (on the electronically excited state), and 13% form the C2 products (on the hot electronic ground state). The observations presented in the work of Trentelman *et al.*<sup>15</sup> suggest that the formation of C3 products is potentially a slow process that requires intersystem crossing (ISC) onto the triplet manifold. However, the proposed photochemical mechanism assumes an  $S_1$  intermediate that survives long enough to undergo

thermalization and, therefore, produce a statistical partitioning of products; this assumption does not necessarily hold given the speed at which  $S_0 \leftarrow S_1$  relaxation is expected to take place. The authors of the work of Kuhlman *et al.*<sup>11,27</sup> have studied the 200 nm photolysis of cyclobutanone, comparatively, associating  $S_1 \leftarrow S_2$  relaxation with two time constants of  $\sim 350$  and  $\sim 750$  fs. Using photoelectron spectroscopy and time-resolved mass spectrometry (TR-MS), the authors were able to resolve two species: the parent ion and a fragment ion with a mass-to-charge ratio  $m/z = 42$  (corresponding to  $H_2C-C=O$ ).<sup>11,27</sup> Both the species exhibited similar electronically excited state decay constants.<sup>11,27</sup> The authors also reported a blue shift in the photoelectron spectrum arising from a coherent oscillatory motion assigned to a low-frequency ( $35$  cm<sup>-1</sup>) cyclobutane ring puckering mode activated by removal of an electron from the carbonyl oxygen  $n$  orbital;<sup>11,27</sup> this process leads to a relaxation of the  $sp^2$  hybridization of the carbonyl carbon due to increased mixing with components of the bonding orbitals in the carbonyl group as well as a relaxation of the adjacent carbon-carbon bonds.

From the perspective of theory, the authors of the work of Xia *et al.*<sup>17</sup> carried out a quantum chemical investigation in order to locate key minima, transition states, and CIs for cyclobutanone, as well as to develop (relaxed) two-dimensional singlet ( $S_1$ ) and triplet ( $T_1$ ) excited state potential energy surfaces using high-level quantum chemical calculations. On the basis of these calculations, the authors of the work of Xia *et al.* proposed that ring opening occurs on the  $S_1$  state through an accessible  $S_1/S_0$  CI.<sup>17</sup> The authors of the work of Liu *et al.*<sup>18</sup> extended this work by performing excited state dynamics simulations under the *ab initio* multiple spawning (AIMS)<sup>28,29</sup> framework following simulated  $S_1 \leftarrow S_0$  photoexcitation. The authors corroborated that  $S_0 \leftarrow S_1$  relaxation occurs primarily through the  $S_1/S_0$  CI located along the  $\alpha$ -cleavage channel; relaxation was observed at geometries where the  $C_{\beta} \approx 1.6$  Å and  $C_{\alpha} \approx 2.5$ – $3.5$  Å.<sup>18</sup> Comparatively, relaxation through CI associated with the formation of C2 products was observed at geometries where  $C_{\beta} \approx 4.0$  Å, although these geometries comprised as little as  $\sim 15\%$  of geometries at which relaxation was observed.<sup>18</sup> The authors reported an excited state lifetime on the  $S_1$  state of  $\sim 500$  fs and, on this basis, proposed that non-ergodic behavior was the driver of the change in C3:C2 product ratio as a function of excitation wavelength.<sup>18</sup> In adopting an alternative approach, the authors of the work of Kuhlman *et al.*<sup>24</sup> developed a four-state, five-dimensional model Hamiltonian and carried out quantum dynamics to study the  $S_1 \leftarrow S_2$  relaxation in cyclobutanone. The authors concluded that  $S_1 \leftarrow S_2$  relaxation is driven by specific nuclear modes (including the cyclobutane ring puckering, carbonyl out-of-plane deformation, symmetric and asymmetric C–CO–C stretches, and carbonyl stretching modes) that couple the  $S_2$  and  $S_1$  states and promote population transfer on the sub-picosecond timescale.<sup>24</sup> While the model presented in the work of Kuhlman *et al.*<sup>24</sup> is informative, their potentials were built within a harmonic normal mode representation and are consequently unable to address satisfactorily large amplitude nuclear motions associated with the formation of fragmentary products.

Despite the concerted efforts of experiment and theory, there remain a significant number of open questions regarding the photochemistry and photochemical dynamics of cyclobutanone that evolve post-photoexcitation to the  $S_2$  Rydberg ( $3s \leftarrow n$ ) state. Nonetheless, the emergence of modern light sources<sup>30,31</sup> is enabling

the study of ultrafast excited state dynamics using both x rays and electrons<sup>32–35</sup> with ever-increasing spatial and temporal resolution; experiments like this are providing the potential for novel and increasingly detailed insights into complex photochemical processes such as these. These developments are driving commensurate progress in theory and are starting to bring into focus a crucial question (which is that posed in the present Special Issue to which this article contributes): *How accurate are modern excited state dynamics simulations really?*

In this article, we combine quantum multiconfigurational time-dependent Hartree (MCTDH) and excited state trajectory surface-hopping dynamics (TSHD) simulations at the density functional [linear-response time-dependent density functional theory (LR-TDDFT)(PBE0)] and algebraic diagrammatic constructor [ADC(2)] levels of theory to explore the relaxation dynamics of cyclobutanone post-photoexcitation to the S<sub>2</sub> Rydberg (3s ← n) state. Our MCTDH and TSHD simulations are subsequently used to predict the scattering signals in an ultrafast electron diffraction (UED) experiment in reciprocal and real space to establish how the complex relaxation dynamics of cyclobutanone might manifest as an experimental observable. In such a UED experiment, free cyclobutanone molecules introduced *in vacuo* will be photoexcited at 200 nm [i.e., into the S<sub>2</sub> Rydberg (3s ← n) state] and probed via electron scattering at a sequence of temporal delays to image directly the evolving excited state structural dynamics.

## II. THEORY AND COMPUTATIONAL DETAILS

### A. Quantum chemistry

All (LR-)TDDFT and ADC(2) quantum chemical calculations were carried out using TURBOMOLE (v7.4).<sup>36,37</sup> The density functional calculations on the electronic ground and excited states used density functional theory (DFT) and linear-response time-dependent DFT (LR-TDDFT), respectively, with the PBE0<sup>38</sup> density functional and the aug-cc-pVDZ<sup>39,40</sup> basis set. The Tamm–Dancoff<sup>41</sup> approximation (TDA) was used throughout. Benchmarks of the level of electronic structure theory and the basis set are available in the supplementary material. Vibrational analysis were performed to confirm the absence of imaginary frequencies at the ground state minimum. All minimum-energy conical intersections (MECIs) were optimized using Turbomole (v7.4) coupled with an external (penalty-function-based) optimizer.<sup>42</sup> Linear interpolation in internal coordinates (LIICs) plots of the potential energy surfaces between critical geometries and these MECI are available in the supplementary material.

Additional quantum chemical calculations were carried out at critical geometries using the second-order algebraic diagrammatic construction scheme [ADC(2)] and *n*-electron valence state perturbation theory (NEVPT2). All ADC(2) calculations were carried out using Turbomole (v7.4),<sup>36,37</sup> all NEVPT2 calculations were carried out using ORCA.<sup>43,44</sup>

### B. Vibronic coupling Hamiltonian and quantum dynamics

The model Hamiltonian is based upon the vibronic coupling approximation<sup>45,46</sup> and is expressed as

$$\mathbf{H} = (T_N + V_0)\mathbf{1} + \mathbf{W}^{dia.} + \mathbf{W}^{SOC}. \quad (1)$$

The electronic diabatic Hamiltonian elements,  $W_{n,m}$ , are obtained by expanding  $\mathbf{W} - V_0\mathbf{1}$ , the diabatic potential, as a Taylor series around a reference nuclear geometry,  $Q_0$ , here taken as the Franck–Condon (e.g., S<sub>0</sub> minimum-energy) geometry.  $V_0$  is a reference potential, here defined as a set of harmonic potentials with vibrational frequencies  $\omega_i$  along dimensionless normal coordinates  $Q_i$ . In this case, the Hamiltonian elements are expressed as

$$W_{n,m} - V_0\delta_{nm} = \varepsilon_n\delta_{nm} + \sum_i^{3N-6} \frac{\partial W_{n,m}}{\partial Q_i} \Big|_{Q_0} \times Q_i + \frac{1}{2!} \sum_{ij}^{3N-6} \frac{\partial^2 W_{n,m}}{\partial Q_i \partial Q_j} \Big|_{Q_0} \times Q_i Q_j + \frac{1}{3!} \frac{\partial^3 W_{n,m}}{\partial Q_i \partial Q_j \partial Q_k} \Big|_{Q_0} Q_i Q_j Q_k + \dots, \quad (2)$$

where  $\delta_{nm}$  is the Kronecker delta.  $Q_i$  denotes the set of  $3N - 6$  dimensionless normal coordinates related to the normal modes of vibration where  $N$  is the number of atoms.  $V_0$ , under the harmonic approximation, is expressed as

$$V_0 = \frac{1}{2} \omega_i Q_i^2 \quad (3)$$

and the kinetic energy operator,  $\hat{T}_N$ , takes the form

$$\hat{T}_N = -\sum_i \frac{1}{2} \omega_i \frac{\partial^2}{\partial Q_i^2}. \quad (4)$$

Due to the anharmonicity of the potential energy surface, the Taylor series expansion is carried out up to fourth order.<sup>47–49</sup> Obtaining the expansion coefficients for the Hamiltonian is simplified for the present system via use of symmetry; the S<sub>0</sub> minimum-energy geometry of cyclobutanone is C<sub>s</sub> symmetric and, consequently, first- and second-order couplings are only allowed so long as the following selection rules are satisfied:

$$\Gamma_n \otimes \Gamma_{Q_a} \otimes \Gamma_n \supset A', \quad (5)$$

$$\Gamma_n \otimes \Gamma_{Q_a} \Gamma_{Q_b} \otimes \Gamma_n \supset A'. \quad (6)$$

All expansion coefficients were obtained using the in-house-developed VCMaker<sup>50,51</sup> software, available at Ref. 52.

The quantum dynamics simulations over the multidimensional potential energy surface(s) were carried out using the MCTDH<sup>53,54</sup> approach as implemented in Quantics.<sup>55</sup> The initial wavefunction for the electronic ground state was built using one-dimensional harmonic oscillator functions with an expectation value of zero momentum along all coordinates; this wavefunction was then projected vertically from the electronic ground state (S<sub>0</sub>) into the S<sub>2</sub> Rydberg (3s ← n) state at the Franck–Condon geometry ( $Q = 0$ ). The complete computational details are available in the supplementary material.

### C. Excited state trajectory surface-hopping dynamics

“On-the-fly” excited state TSHD simulations were carried out using Newton-X (v2.4).<sup>56,57</sup> All potential energy surfaces,

derivatives, and respective couplings were computed using Turbomole (v7.4)<sup>36,37</sup> at two separate levels of theory [LR-TDDFT(PBE0) and ADC(2)] in two separate sets of simulations. Trajectories were propagated using the velocity Verlet algorithm<sup>58,59</sup> for a maximum time of 5 ps ( $t_{\max} = 5000$  fs) with a time step of 0.5 fs ( $dt = 0.5$  fs). The state-to-state transitions (or “hops”) were simulated using the Hammes-Schiffer-and-Tully fewest-switches algorithm<sup>60</sup> with the state-to-state couplings estimated via the time-dependent Baek–An<sup>61</sup> scheme. The excited state TSHD simulations were initiated by vertical projection of a set of initial conditions, generated according to a Wigner distribution with a temperature of 100 K, from the electronic ground state ( $S_0$ ) into the  $S_2$  Rydberg ( $3s \leftarrow n$ ) state.

To avoid instabilities at/around the  $S_1/S_0$  crossing seam,  $S_0 \leftarrow S_1$  surface hops were forced when the  $S_1/S_0$  energy gap fulfilled the criterion  $\Delta E_{S_1-S_0} < 0.1$  eV.

#### D. Electron diffraction simulations

Throughout this article, we present UED scattering signals as modified electron scattering intensities,  $sM(\mathbf{s})$ , as computed under the independent atom model (IAM). This presentation is used to enhance the oscillations in the UED scattering signal associated with the molecular interference terms,  $I_{\text{mol}}(\mathbf{s})$ , and suppress the rapid drop-off in UED scattering signal as a function of the scattering vector,  $\mathbf{s}$ , arising from the elastic scattering amplitude.  $sM(\mathbf{s})$  is given by

$$sM(\mathbf{s}) = \frac{I_{\text{mol}}(\mathbf{s})}{I_{\text{at}}(\mathbf{s})} \mathbf{s}, \quad (7)$$

where  $\mathbf{s}$  is the momentum transfer, or scattering, vector.  $I_{\text{at}}(\mathbf{s})$  is the atomic scattering term, given by

$$I_{\text{at}}(\mathbf{s}) = \sum_i^N |f_i(\mathbf{s})|^2, \quad (8)$$

and  $I_{\text{mol}}(\mathbf{s})$  is the molecular scattering term, expressed as a sum over interference terms, given by

$$I_{\text{mol}}(\mathbf{s}) = \sum_i^N \sum_{j \neq i}^N |f_i(\mathbf{s})| |f_j(\mathbf{s})| \frac{\sin(\mathbf{s}r_{ij})}{\mathbf{s}r_{ij}}, \quad (9)$$

where  $f_i(\mathbf{s})$  and  $f_j(\mathbf{s})$  are the elastic scattering amplitudes for atoms  $i$  and  $j$ , respectively, and  $r_{ij}$  is the internuclear distance between atoms  $i$  and  $j$ .

$sM(\mathbf{s})$  can be transformed into a pair-distribution function (PDF; i.e., from reciprocal space into real space) using a sine transformation:

$$\text{PDF}(\mathbf{r}) = \int_0^{s_{\max}} sM(\mathbf{s}) \sin(\mathbf{s}\mathbf{r}) e^{-k\mathbf{s}^2} ds, \quad (10)$$

where  $s_{\max}$  is the maximum momentum transfer in the data,  $r$  is the internuclear distance between atom pairs, and  $k$  is a damping factor used to drive down smoothly the contribution(s) at high  $s$  to zero. A damping factor of  $k = 0.03$  was used throughout this article.

The focus of this work is upon the ultrafast excited state dynamics of cyclobutanone and, accordingly, the ultrafast electron diffraction scattering signal is presented as a transient (i.e., as an excited state – ground state “difference”) signal where appropriate under the nuclear ensemble model. The ground state signal used to generate the transient is predicted from the trajectory surface-hopping dynamics initial conditions, i.e., the nuclear ensemble representing the state of the system at  $t = 0$ . No scaling for, e.g., excitation percentage/photolysis yield has been carried out.

### III. RESULTS

#### A. Characterizing critical points on the ground- and electronically excited potential energy surfaces

Table I shows the energies of the low-lying singlet ( $S_n$ ;  $n = [1, \dots, 5]$ ) and triplet ( $T_n$ ;  $n = [1, \dots, 5]$ ) electronically excited states of cyclobutanone. Figure S1 shows the molecular orbitals involved in the electronic transitions. The symmetry point group of cyclobutanone ( $C_s$  at the  $S_0$  minimum-energy geometry) is used to characterize the symmetries of the electronically excited states (an important facet of the generation and interpretation of the model Hamiltonian used in Sec. III B).

At the  $S_0$  minimum-energy geometry, the  $S_1$  and  $S_2$  excited states are located (1) 4.21 and 5.99 eV, respectively, above the electronic ground state at the ADC(2)/aug-cc-pVTZ level of theory and (2) 4.33 and 6.10 eV, respectively, above the electronic ground state at the LR-TDDFT(PBE0)/aug-cc-pVDZ level of theory. Both levels of theory give good agreement with the experimental absorption spectrum recorded in the work of Diao *et al.*<sup>10</sup> in which absorption bands are observed at  $\sim 4.2$  and  $\sim 6.2$  eV. At both levels of theory, the  $S_1$  and  $S_2$  states have  $\pi^* \leftarrow n$  (LUMO  $\leftarrow$  HOMO) and  $3s \leftarrow n$

**TABLE I.** Summary of electronic energies, characters, and symmetries of the ground- (GS) and electronically excited ( $S_n/T_n$ ;  $n = [1, \dots, 5]$ ) states of cyclobutanone evaluated at the  $S_0$  minimum-energy geometry and at the ADC(2)/aug-cc-pVTZ and LR-TDDFT(PBE0)/aug-cc-pVDZ levels of theory. Comparative tables for evaluations at the  $S_1$ - (Table S3) and  $S_2$ -state (Table S4) minimum-energy geometries are presented in the supplementary material. The relevant molecular orbitals are shown in the supplementary material. The HOMO is designated as H; the LUMO is designated as L.

State	ADC(2)		LR-TDDFT(PBE0)	
	Energy/eV	Character (Irrep.)	Energy/eV	Character (Irrep.)
GS	0.00	— ( $A'$ )	0.00	— ( $A'$ )
$S_1$	4.21	H $\rightarrow$ L ( $A''$ )	4.33	H $\rightarrow$ L ( $A''$ )
$S_2$	5.99	H $\rightarrow$ L+1 ( $A''$ )	6.10	H $\rightarrow$ L+1 ( $A''$ )
$S_3$	6.53	H $\rightarrow$ L+3 ( $A''$ )	6.67	H $\rightarrow$ L+3 ( $A''$ )
$S_4$	6.64	H $\rightarrow$ L+2 ( $A'$ )	6.77	H $\rightarrow$ L+2 ( $A'$ )
$S_5$	6.68	H $\rightarrow$ L+4 ( $A''$ )	6.78	H $\rightarrow$ L+4 ( $A''$ )
$T_1$	3.87	H $\rightarrow$ L ( $A''$ )	3.73	H $\rightarrow$ L ( $A''$ )
$T_2$	5.95	H-1 $\rightarrow$ L ( $A'$ )	5.98	H-1 $\rightarrow$ L ( $A'$ )
		H-4 $\rightarrow$ L		H-4 $\rightarrow$ L
$T_3$	6.32	H $\rightarrow$ L+1 ( $A''$ )	6.02	H $\rightarrow$ L+1 ( $A''$ )
$T_4$	6.50	H $\rightarrow$ L+3 ( $A''$ )	6.61	H $\rightarrow$ L+3 ( $A''$ )
$T_5$	6.62	H $\rightarrow$ L+2 ( $A'$ )	6.63	H $\rightarrow$ L+2 ( $A'$ )

(LUMO + 1  $\leftarrow$  HOMO) character, respectively. The Rydberg character of the  $S_2$  state requires a larger basis set to describe accurately its energy and electronic structure, while—in contrast—the valence  $S_1$  state exhibits little to no dependence on basis set (Table S1). Both the  $S_2$  and  $S_1$  states are of  $A''$  symmetry; direct first-order vibronic coupling between these two states is consequently forbidden, and this can be expected to slow down the rate of internal conversion (IC) between the two states.

The ADC(2) calculations give good agreement with the experimentally observed ordering and energies of the electronic states at the Franck–Condon geometry. However, previous work<sup>62</sup> has highlighted a limitation of the ADC(2) approach for studying non-radiative relaxation pathways of carbonyl-containing molecules as it has a tendency to predict artificial  $S_1/S_0$  crossings along the carbonyl stretching coordinate. These artificial  $S_1/S_0$  crossings arise from (i) a  $\pi^* \leftarrow n$  potential that is too shallow combined with (ii) a ground state potential that destabilizes too rapidly. To demonstrate this, we present calculations of the two potentials along the carbonyl stretching mode in Fig. S2 at the LR-TDDFT(PBE0), ADC(2), and NEVPT2(12,12) levels of theory. Figure S2 indicates good agreement on the form of the potentials between the LR-TDDFT(PBE0) and NEVPT2(12,12) levels of theory: Although the ground state and  $\pi^* \leftarrow n$  surfaces come closer in energy, they do not cross. In contrast, and as expected from Ref. 62, there is a clear (and artificial)  $S_1/S_0$  crossing between the two potentials at the ADC(2) level of theory occurring at a C=O bond length of  $\approx 1.6$  Å. This low-lying (i.e., accessible)  $S_1/S_0$  crossing point is likely to distort the excited state dynamics crossing from the  $S_1$  to ground state surface and indeed such dynamics are presented in the supplementary material.

The  $S_1$ -state minimum-energy geometry is reached from the Franck–Condon point via out-of-plane puckering of the cyclobutane ring and a slight elongation of the C=O bond (1.21–1.26 Å); the carbon–carbon bonds in the cyclobutane ring ( $C_\alpha$  and  $C_\beta$ ) remain almost unchanged. These structural changes destabilize the electronic ground state (Table S3); it is increased in energy by 1.13 eV relative to the  $S_0$ -state minimum-energy geometry at the LR-TDDFT(PBE0)/aug-cc-pVDZ level of theory. In contrast, the  $S_1$  ( $\pi^* \leftarrow n$ ) state is stabilized, decreasing the energy gap with the  $S_0$  state while increasing the gap with the higher-lying singlet states ( $S_n$ ;  $n > 1$ ). The predicted emission energy from the  $S_1$  minimum-energy geometry is  $\sim 3.9$  eV, a value that is in excellent agreement with the emission spectrum recorded in the work of Lee *et al.*<sup>63</sup> The broad band observed in the absorption spectrum recorded in the work of Diau *et al.*<sup>10</sup> is consistent with a short-lived electronically excited state, however, which is indicative of competitive photochemical channels, e.g., non-radiative decay on the

femto/picosecond timescale through accessible CIs as discussed by Liu and Fang.<sup>18</sup>

The  $S_2$ -state minimum-energy geometry (Table S4), in contrast, is reached from the Franck–Condon point via contraction of the C=O bond (1.21–1.16 Å) and slight elongation of the carbon–carbon bonds in the cyclobutane ring ( $C_\alpha$  and  $C_\beta$ ). The effect of these structural changes is a destabilization of the ground and  $S_1$  states; the  $S_0$  state increases in energy by 0.51 eV with a similar (0.58 eV) increase observed for the  $S_1$  state at the LR-TDDFT(PBE0)/aug-cc-pVDZ level of theory. The absorption spectrum for excitation into this state exhibits a distinct vibronic structure suggestive of both a longer-lived electronically excited state and the activation of vibrational modes on excitation.<sup>10</sup>

Previous studies, e.g., that of Kao *et al.*,<sup>3</sup> have hypothesized as to the potential role of triplet states in the photochemistry of cyclobutanone; this is our motivation for presenting the details of these states ( $T_n$ ;  $n = [1, \dots, 5]$ ) in Table I and the relevant state-to-state spin–orbit couplings (SOCs) in the supplementary material (Table S7). At the Franck–Condon geometry, the lowest-energy electronically excited triplet state ( $T_1$ ) is located at 3.73 eV above the electronic ground state at the LR-TDDFT(PBE0)/aug-cc-pVDZ level of theory and is of the same  $\pi^* \leftarrow n$  character as the  $S_1$  state; consequently,  $S_1/T_1$  SOC will be formally forbidden.<sup>64,65</sup> The  $T_2$  and  $T_3$  states are near-degenerate and located a little under the  $S_2$  (6.10 eV) at 5.98 and 6.02 eV, respectively, above the electronic ground state at the LR-TDDFT(PBE0)/aug-cc-pVDZ level of theory. The SOC between these triplet states and the low-lying singlet electronically excited states is generally small (Table S7), suggesting that the triplet states are unlikely to play a significant role in the early-time (e.g.,  $< 2$  ps) channels.

Figure 2(b) shows the structure of an  $S_2/S_1$  MECI, while Figs. 2(c)–2(e) show the structures of three  $S_1/S_0$  MECI as located via penalty-function-constrained optimization at the LR-TDDFT(PBE0)/aug-cc-pVDZ level of theory. Cartesian coordinates are given in the supplementary material. Potential energy surfaces between the Franck–Condon point and each of the  $S_1/S_0$  MECI were calculated via linear interpolation in internal coordinates (LIICs) at the LR-TDDFT(PBE0)/aug-cc-pVDZ level of theory, and these are also given in the supplementary material.

The  $S_2/S_1$  MECI [Fig. 2(b)] is located 5.85 eV above the  $S_0$  minimum-energy geometry, i.e.,  $\sim 0.5$  eV below the  $3s \leftarrow n$  excitation energy, at the LR-TDDFT(PBE0)/aug-cc-pVDZ level of theory. Its structure is similar to the Franck–Condon geometry although it features a symmetry-breaking distortion of the cyclobutane ring [seen clearly on inspection of the position of the hydrogen atoms in Fig. 2(b)]. The potential energy surface between the

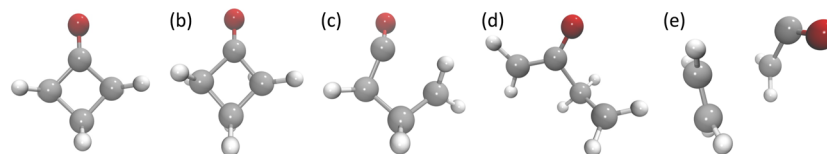


**FIG. 2.** Key geometries of cyclobutanone: (a) the  $S_0$  minimum-energy geometry, (b) the (symmetry-broken)  $S_2/S_1$  MECI, and the  $S_1/S_0$  (c)  $C_\alpha$ -cleavage, (d)  $C_\beta$ -cleavage, and (e)  $C_\alpha$ - $C_\beta$ -cleavage MECIs. All geometries were optimized at the LR-TDDFT(PBE0)/aug-cc-pVDZ level of theory.

Franck–Condon geometry and this  $S_2/S_1$  MECI is barrierless at LR-TDDFT(PBE0)/aug-cc-pVDZ level of theory (Fig. S3), which would suggest that  $S_2/S_1$  internal conversion should be (ultra)fast in the absence of any additional considerations. However, the symmetries of the two states at the Franck–Condon geometry are such that the interstate coupling is forbidden; even at the distorted  $S_2/S_1$  MECI geometry, it is weak and results predictably in a longer lifetime for the  $S_2$  state.

The three  $S_1/S_0$  MECIs [Figs. 2(c)–2(e)] are located in qualitative agreement (geometrically and energetically) with those reported by Liu and Fang<sup>18</sup> [located by the authors at the complete active space self-consistent field (CASSCF) level of theory]. The first [Fig. 2(c)] one is located along the  $\alpha$ -cleavage channel, the second [Fig. 2(d)] along the  $\beta$ -cleavage channel, and the third [Fig. 2(e)] along a concerted  $\alpha/\beta$ -cleavage channel. The energetic ordering of the three  $S_1/S_0$  MECIs (3.40, 2.56, and 5.0 eV, respectively, above the  $S_0$  minimum-energy geometry at the LR-TDDFT(PBE0)/aug-cc-pVDZ level of theory) follows qualitatively the trend observed for the three  $S_1/S_0$  MECIs in Ref. 18, although it is important to note that the single-reference nature of LR-TDDFT(PBE0) favors charged rather than biradical dissociation along the  $\alpha$ - and  $\beta$ -cleavage channels and, furthermore, renders it unable to describe properly the topology/dimensionality of the  $S_1/S_0$  crossing seam. Although all of the  $S_1/S_0$  MECIs are energetically accessible, i.e., they and their barriers are submerged relative to the  $\sim 6.2$  eV excitation energy, the description of the potential energy surface around the  $S_1/S_0$  MECIs is likely to be problematic for LR-TDDFT(PBE0) and it is quite possible that this might affect product production by influencing the dynamics through and in the vicinity of the MECI and, subsequently, the motion of the trajectory/wavepacket on the electronic ground state potential energy surface.

Overcoming these aforementioned limitations could be achieved using a multireference (active space) method, e.g., CASSCF/CASPT2 or NEVPT2, for the excited state TSHD simulations. However, the performance of this family of methods is greatly dependent on the choice of active space; an appropriate active space should be large enough to incorporate all of the orbitals required over all of the nuclear configurations explored in the TSHD simulations while not too large so as to render the TSHD simulations computationally costly to the point of intractability. We found an active space of eight electrons in eight orbitals [e.g., NEVPT2(8,8)] unstable with respect to orbital rotation(s) at some geometries (particularly those where the cyclobutane ring was distorted), while a larger active space of 12 electrons in 12 orbitals [e.g., NEVPT2(12,12)] was too computationally expensive to carry out practically TSHD simulations. Consequently, we elected to carry out our excited state TSHD simulations at the LR-TDDFT(PBE0)/aug-cc-pVDZ level of theory, keeping in mind the aforementioned (although well-understood) limitations and their potential impact on the dynamics (which we discuss in detail). However, we note within the context of the present challenge that other contributors have performed excited state dynamics simulations with multireference (active space) methods, e.g., CASSCF based on an eight-electron-in-eleven-orbital active space<sup>66</sup> and extended multistate CASPT2 (XMS-CASPT2) based on an eight-electron-in-eight-orbital active space.<sup>67</sup>

## B. Early-time dynamics using a spin-vibronic coupling Hamiltonian

To (i) identify possible photochemical (fragmentation) channels, (ii) clarify the potential involvement of triplet states, and (iii) establish a mechanism for internal conversion from the initially excited  $S_2$  ( $3s \leftarrow n$ ) state to the lowest-energy singlet electronically excited state ( $S_1$ ) at early times, we developed a model Hamiltonian and carried out MCTDH simulations. The model Hamiltonian comprised the electronic ground state ( $S_0$ ) and nine electronically excited states [four singlets ( $S_n$ ;  $n = [1, \dots, 4]$ ) and five triplets ( $T_n$ ;  $n = [1, \dots, 5]$ )]. The inclusion of singlet states higher in energy than the  $S_2$  (e.g.,  $S_n$ ;  $n > 2$ ) is motivated by the absence of vibronic coupling between the  $S_1$  and  $S_2$  states, both of which are of  $A''$  symmetry (Table I); here, coupling to higher-lying singlet states of, e.g., alternative symmetries offers the potential of second-order population transfer channels comparable to those identified in other systems where direct population transfer channels are weak or otherwise absent.<sup>68–70</sup>

The model Hamiltonian incorporated eight degrees of vibrational freedom in nuclear configurational space:  $\nu_1$ ,  $\nu_7$ ,  $\nu_{10}$ ,  $\nu_{11}$ ,  $\nu_{12}$ ,  $\nu_{13}$ ,  $\nu_{15}$ , and  $\nu_{21}$ , which were selected on the basis of the magnitude of their first-order couplings and the symmetries of the vibrational modes. The degrees of vibrational freedom included in the model Hamiltonian comprised cyclobutane ring puckering ( $\nu_1$  and  $\nu_{12}$ ), symmetric and antisymmetric cyclobutane ring breathing ( $\nu_7$  and  $\nu_{10}$ ), cyclobutane ring deformation ( $\nu_{11}$ ,  $\nu_{13}$  and  $\nu_{15}$ ), and the carbonyl stretching mode ( $\nu_{21}$ ), for consistency with previous work, e.g., that of Kuhlman *et al.*<sup>11</sup> To assess the approximate accuracy of our model Hamiltonian, we present Fig. 3, which compares the experimental<sup>10</sup> and theoretical absorption spectrum for the  $S_2$  state. There is excellent agreement between the two absorption spectra, supporting the assertion that our model Hamiltonian describes accurately the (local) potential energy surface(s). The absorption spectra in Fig. 3 feature a vibrational progression with structured

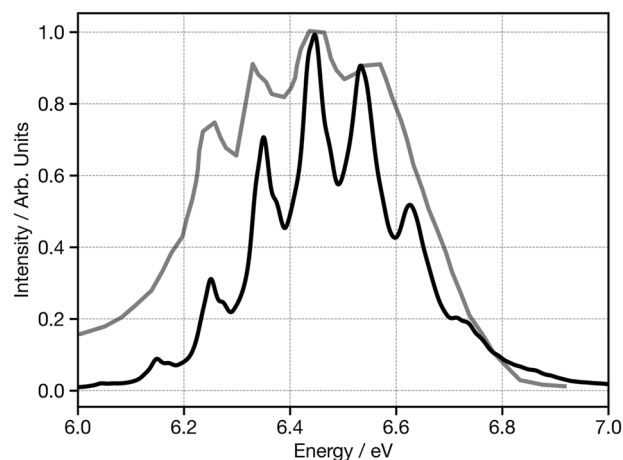


**FIG. 3.** Theoretical (black) and experimental (gray)  $S_2 \leftarrow S_0$  ( $3s \leftarrow n$ ) absorption spectrum. The theoretical spectrum is shown shifted by  $\Delta E = +0.14$  eV. The experimental spectrum was recorded in the work of Diau *et al.* and is provided in digitized from Ref. 10.

peaks separated by  $\sim 0.1$  eV (consistent with the carbonyl out-of-plane wagging and cyclobutane ring puckering vibrational modes previously identified<sup>71</sup> and arising, in the present model, via the inclusion of  $\nu_{12}$  into the model Hamiltonian).

Figure 4 shows the transfer of population from the  $S_2$  state over 600 fs post-photoexcitation into the  $S_2$  ( $3s \leftarrow n$ ) state as computed via quantum dynamics. The  $S_1 \leftarrow S_2$  population transfer occurs at a rate of  $\sim 1.67 \times 10^{-12} \text{ s}^{-1}$  with the  $S_1$  state population exceeding  $S_2$  within  $\sim 350$  fs. This is qualitatively consistent with the decay of the peak associated with the  $S_2$  state in the photoelectron spectrum recorded in the work of Kuhlman *et al.*<sup>11</sup> (the authors report a biexponential fit yielding time constants of  $\sim 350$  and 750 fs). The  $S_1 \leftarrow S_2$  population transfer in the model Hamiltonian obtains intensity via mixing with the higher-lying singlet electronically excited states, especially the  $S_4$  state (the lowest-lying singlet electronically excited state of  $A'$  character). This occurs most prominently along  $\nu_{11}$ . While this mode is responsible for the state-to-state coupling, it is  $\nu_1$ ,  $\nu_{12}$ ,  $\nu_{13}$ , and  $\nu_{21}$  that exhibit the largest-amplitude nuclear oscillations and electronically excited state structural changes that are likely to be observed in the ultrafast electron diffraction experiment. The population oscillations observed between the  $S_2$  and  $S_1$  states are associated with the overcoherence of the reduced model Hamiltonian and are, in any case, faster than the temporal resolution of the ultrafast electron diffraction experiments.

$S_0 \leftarrow S_1$  population transfer is not included in the present model Hamiltonian. The high energy of the  $S_2$  state results in an exceptionally hot wavefunction on the electronic ground state that is difficult to converge under the framework of the quantum dynamics simulations. In addition, previous works—and our own quantum chemical calculations—have identified  $S_1/S_0$  MECI at highly distorted geometries beyond the limits of the normal model representation on which the quantum dynamics simulations are predicated (the representation is only valid to small distortions from the equilibrium, e.g.,  $S_0$  minimum-energy, geometry). Consequently, to describe more completely the excited state relaxation

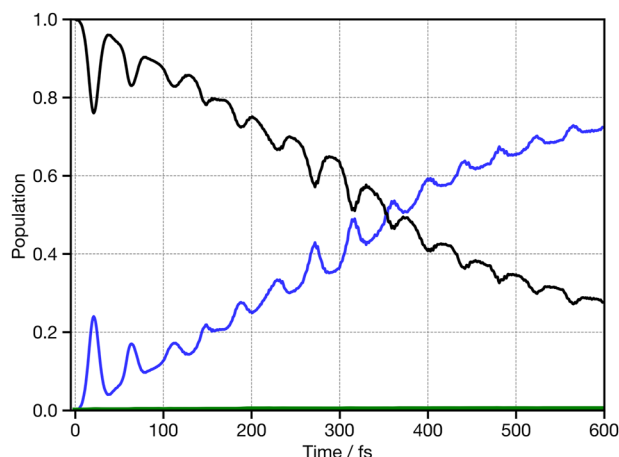


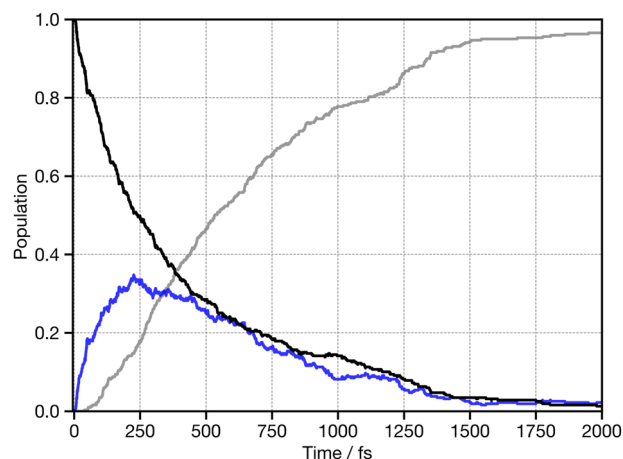
**FIG. 4.** Population kinetics obtained from quantum dynamics simulations over 600 fs post-photoexcitation into the  $S_2$  ( $3s \leftarrow n$ ) state. The  $S_2$  state population is shown in black; the  $S_1$  state population is shown in blue; the triplet ( $T_n$ ;  $n = [1, \dots, 5]$ ) state populations are shown (collectively) in green.

dynamics, we explore excited state molecular dynamics simulations operating in unconstrained nuclear configurational space through the trajectory surface-hopping approach.

### C. Excited state relaxation dynamics in unconstrained nuclear configuration space using trajectory surface-hopping dynamics

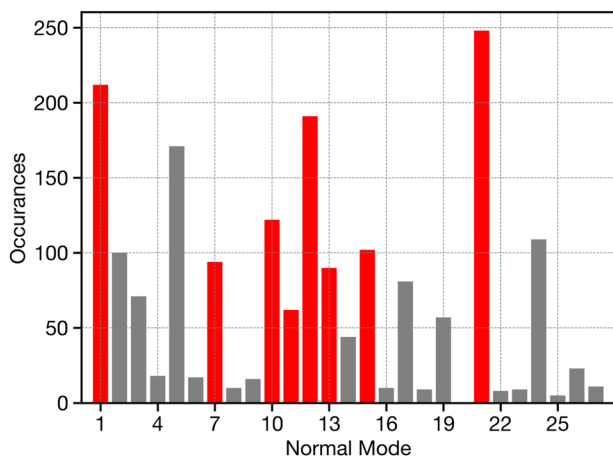
Figure 5 shows the populations of the  $S_2$ ,  $S_1$ , and  $S_0$  states over the first 2 ps post-photoexcitation into the  $S_2$  ( $3s \leftarrow n$ ) state as obtained from 289 *on-the-fly* surface-hopping trajectories propagated at LR-TDDFT(PBE0)/aug-cc-pVDZ level of theory. A similar set of trajectory surface-hopping dynamics propagated at the ADC(2)/aug-cc-pVDZ level of theory are presented and analyzed in the supplementary material and are of comparative interest. Figure 5 shows  $S_1 \leftarrow S_2$  population transfer with a decay constant of  $\sim 356$  fs. This is slightly faster than observed in the quantum dynamics simulations, i.e., 50% of population decays from  $S_2$  in 225 fs, which is due to the inclusion of the ground state to which the wavepacket can rapidly decay. This decay constant is in close agreement with the fastest time-constant extracted from a photoelectron spectroscopic study,<sup>11</sup> but we do not see any dynamics associated with the  $\sim 700$  fs component reported. Interestingly, this slower component is in close agreement with the population kinetics for the dynamics performed using potentials calculated at ADC(2) level of theory, shown in the supplementary material.

While the timescales between the quantum dynamics and TSH simulations suggest similar dynamics, further analysis is required to assess this in more detail. To achieve this, we transform the first 500 fs of excited state molecular dynamics from Cartesian coordinates into a normal mode representation similar to Ref. 72. Figure 6 shows the normal modes active during the TSH simulations as a bar chart of the number of times each normal mode features in the top 6 of the largest displacements during a trajectory's excited state dynamics. The red bars represent those normal modes included in the model Hamiltonian. This shows close agreement between the



**FIG. 5.** Population kinetics obtained from 289 *on-the-fly* surface-hopping trajectories over 2 ps post-photoexcitation into the  $S_2$  ( $3s \leftarrow n$ ) state. The  $S_2$  state population is shown in black; the  $S_1$  state population is shown in blue; the  $S_0$  state population is shown in gray.

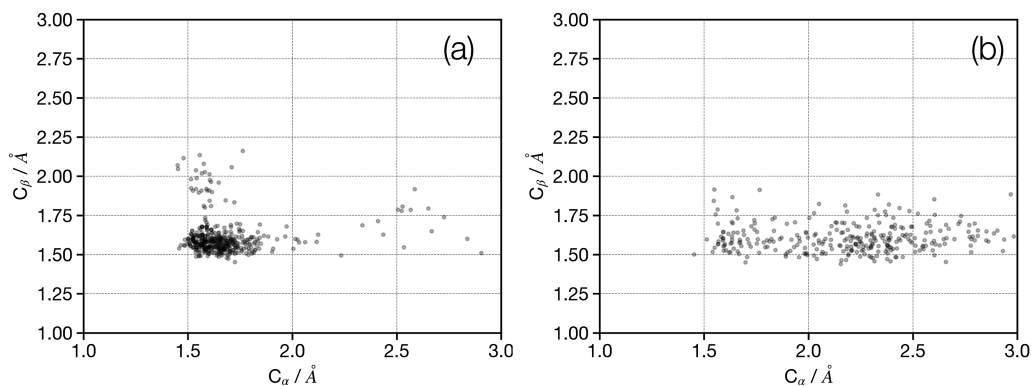




**FIG. 6.** Bar chart showing the number of times that each normal mode features in the top six largest displacements for an (electronically excited state) trajectory. The red bars represent those normal modes included in the model Hamiltonian.

modes that appear most frequently in the TSH simulations and those included in the quantum dynamics. The most notable exception is  $\nu_5$ , which exhibits larger amplitude motion due to the flat nature of the potential but does not act as either tuning or coupling mode and therefore does not strongly influence the excited state dynamics.

Figure 7 shows average  $C_\alpha$  and  $C_\beta$  bond lengths for the structures where each trajectory hops from the  $S_2$ - $S_1$  (a) and  $S_1$ - $S_0$  (b) states. For the former, there is a clear cluster around 1.5–1.6 Å consistent with the ground state structure and therefore close to the Franck–Condon geometry, as expected from the optimized  $S_2/S_1$  discussed above. In contrast, for the  $S_1$ - $S_0$  hopping geometries, there is a significant change, with the majority of hops occurring for  $C_\alpha$  bond lengths  $>2.2$  Å. Using the geometries provided in the supplementary material, the  $C_\alpha$  CI occurs when the  $C_\alpha$  bond length is 2.35 Å, with very little corresponding change along the  $C_\beta$  bond. This suggests, in agreement with previous work, that crossing from the  $S_1$ - $S_0$  occurs primarily at the CI exhibiting a  $C_\alpha$  bond break.



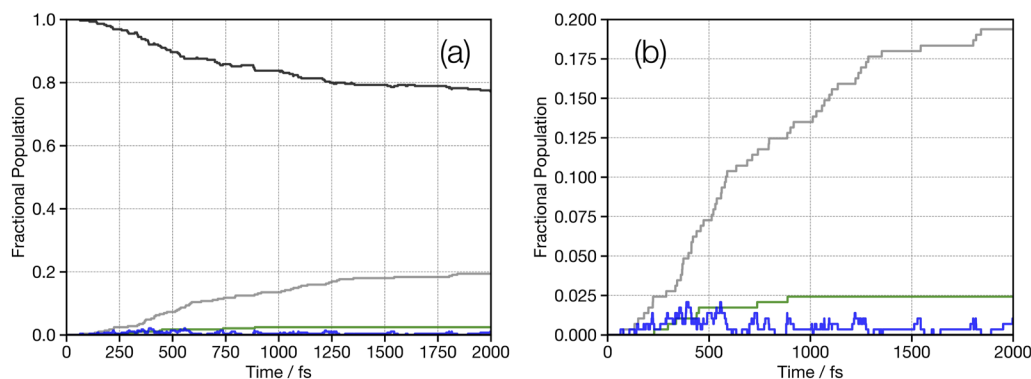
**FIG. 7.** Average  $C_\alpha$  and  $C_\beta$  bond lengths at (a)  $S_1 \leftarrow S_2$  and (b)  $S_0 \leftarrow S_1$  surface-hopping events.

Figure 8 shows the fractional population of the photoproducts formed from the TSH trajectories. This indicates  $\sim 20\%$  of the excited states form the  $C_2H_4 + CH_2CO$ , i.e., decay via the C2 channel, while 2.5% forms the C3 products. The ring-open species are formed, but are very short-lived and either contribute forming either the C2 or C3 products or undergo bond reformation to form vibrationally excited ground state cyclobutanone. The formation of C2 is comparable to but lower than other excited state dynamics simulations performed at a higher level of theory reported in Ref. 67 (34%) and by the authors of the work of Trentelman *et al.*<sup>15</sup> who reported 43% of yield experimentally. The major discrepancy in our simulations occurs for the C3 channels, which is  $>60\%$  in these previous works. The near-absence of the C3 channel is associated with the multireference character of the potential in this region and the bias of single reference methods for charged rather than biradical bond breaking. While this does not significantly increase the energies of the  $C_\alpha$  and  $C_\beta$  CIs (see Fig. S4), it does increase the energy of the double bond breaking CI, making the formation of the C3 channel challenging. To assess this, we also perform dynamics using trajectories in the  $T_1$  state, performed using unrestricted Kohn–Sham facilitating the description of biradical character. These were initiated at random from trajectories populating the  $S_1$  state. Importantly, these show a much higher formation of C3 photoproducts (C3: 53%, C2: 5% and ring-open: 17%) consistent with previous experiments.<sup>15</sup>

#### D. Electron diffraction simulations

Figure 9 shows the time-resolved electron diffraction simulations arising after photoexcitation of cyclobutanone into the  $S_2$  state. Figure 9(a) shows the electron diffraction scattering signal as calculated, while Fig. 9(b) is convolved along the temporal axis with a Gaussian kernel (FWHM = 150 fs) to reproduce the effect(s) of the finite temporal resolution of the proposed electron diffraction experiment. Figures 9(c) and 9(d) show time-resolved pair-distribution function (PDF) maps with and without temporal broadening, respectively, and were produced via sine transformation of the modified scattering intensity maps in Figs. 9(a) and 9(b), respectively.

The modified scattering intensity maps [Figs. 9(a) and 9(b)] show two strong negative ( $\sim 1$  and  $9 \text{ \AA}^{-1}$ ) and two positive ( $\sim 2.7$  and



**FIG. 8.** Fractional population of the photoproducts obtained from the 289 trajectories. (a) Shows all photoproducts, including cyclobutanone (black trace). (b) Zooms into the lower probability photoproducts including the gray trace, which shows the C2 products ( $C_2H_4 + CH_2CO$ ), the green trace, which shows the C3 products ( $C_3H_6 + CO$ ), and the blue trace, which shows ring-opened structures.

$7.5 \text{ \AA}^{-1}$ ) features but do not reveal the richness of the dynamics that reflect the complex photochemistry of cyclobutanone, in part due to the incoherent/stochastic nature of the photochemical processes taking place.

A deeper understanding of the structural changes can be established from Figs. 9(c) and 9(d), which show the time-resolved PDF. For clarity, Fig. 10 shows the PDF( $t = 0$  fs), PDF( $t = 2000$  fs), and the  $\Delta$ PDF( $t = 2000$  fs). The PDF acquired for the 289 initial conditions

exhibits three peaks at  $\sim 1.5$ ,  $\sim 2.5$ , and  $\sim 3.0 \text{ \AA}$ . The first corresponds to the neighboring C–C and C=O distances, the second corresponds to C–C distance on the opposite side of the cycle, and the final peak corresponds to the C–O distances, which are not directly bonded. The transient indicates primarily a loss of the first two peaks associated with dissociation and the formation of the C2 products. We note here that despite the aforementioned differences in the photoproduct formation, the transient scattering and PDFs are very

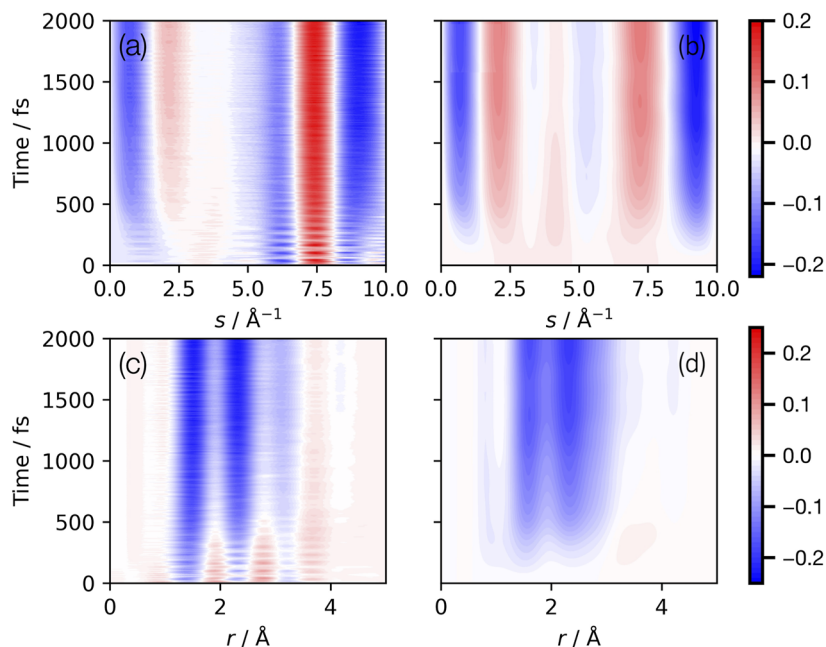


**FIG. 9.** Transient ( $\Delta I/I$ ) scattering (a) without and (b) with 150 fs (FWHM) temporal broadening. Transient PDF (c) without and (d) with 150 fs (FWHM) temporal broadening. The ground state (pre-photoexcitation) signal used to generate the transient signal was obtained from the trajectory surface-hopping dynamics initial conditions, i.e., the nuclear ensemble representing the state of the system at  $t = 0$ . All plots were produced using the 289 2000 fs trajectories simulated at the LR-TDDFT(PBE0)/aug-cc-pVDZ level of theory.

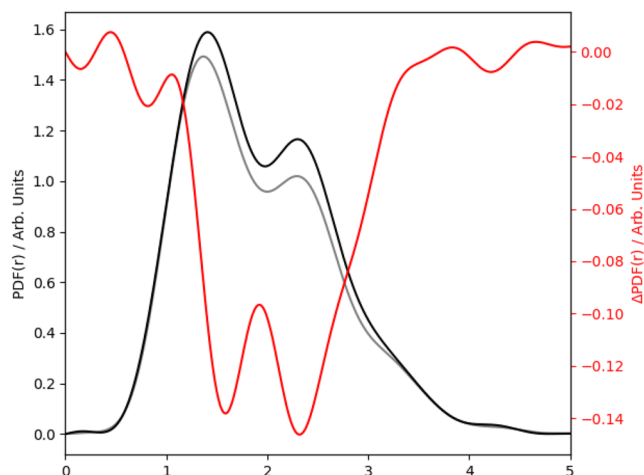


**FIG. 10.** Initial ( $t = 0$  fs; black) and final ( $t = 2000$  fs; gray) PDFs and the difference PDF (red) calculated using the 289 000 fs surface-hopping trajectories simulated using potentials at LR-TDDFT(PBE0) level of theory.

similar to those in Ref. 67. This highlights the challenge in disentangling the exact photoproduct formation of these systems due to the overlapping bands.

#### IV. DISCUSSION AND CONCLUSIONS

In this work, we have carried out quantum and excited state trajectory surface-hopping molecular dynamics simulations to study the electronically excited state relaxation mechanisms and electronic ground state dynamics of cyclobutanone post-photoexcitation into the  $S_2$  Rydberg ( $3s \leftarrow n$ ) state. Our focus has been upon translating these simulations to predict the experimental observables associated with the ultrafast electron diffraction experiments and ultimately to answer the question: *Can excited state dynamics simulations be predictive?* However, even for small molecules such as cyclobutanone, certain approximations in the underlying computational chemical methods are required, which will influence the outcome of such simulations: We highlight this in comparison between the present work and other works related to the same challenge.<sup>66,67,73–83</sup> Consequently, in this section we discuss the relaxation mechanism observed in our simulations as well as potential sources of error and how we expect that these will influence interpretation of the experimental observables.

Within this challenge, the objective has been to translate excited state dynamics into experimental observables. The importance of this cannot be understated. In many cases, collaboration between experimental and theoretical studies focuses upon the comparison of quantities that are easy to calculate, such as electronic state population kinetics. These kinetics are then compared to experimentally extracted timescales and agreement is taken as accuracy of the simulations. However, as shown in this work the LR-TDDFT (356 fs) and XMS-CASPT2<sup>67</sup> (335 fs) dynamics provide very similar decay kinetics but different predictions of photoproducts influencing the experimental signal. While slightly slower, the excited state dynamics performed using ADC(2) potentials also occurs on a comparable timescale ( $\sim 700$  fs), but owing to the artificial crossing along the

C=O bond stretch,<sup>62</sup> the excited state decay occurs via a completely different mechanism.

This highlights one of the key choices that has to be made for any excited state dynamics simulation, i.e., the electronic structure method to simulate the excited state potentials. As discussed above, the single reference methods used in both this LR-TDDFT and ADC(2) exhibit challenges in describing the dynamics between electronically excited states and the ground state. While multireference methods such as CASPT2 will overcome these limitations, this gives rise to a significant computational burden, which, while possible for small molecules such as cyclobutanone, would be prohibitive for larger systems. In addition, their performance strongly depends on the choice of the active space, which is likely to be dynamic, i.e., it changes during the excited state dynamics, necessitating the use of a larger active space. Active space methods without perturbation theory, such as CASSCF, reduce the computational expense, but they do not treat dynamic correlation effects. While the influence of this will be system specific, for cyclobutanone this appears to speed up the excited state decay.<sup>66,77</sup>

Our simulations indicate that after excitation of the  $3s \leftarrow n$  Rydberg state, the system relaxes within 1–2 ps to form a broad range of photoproducts. Decay of this initially excited  $S_2$  state occurs with a time constant of  $\sim 350$  fs. This is in good agreement with the fastest kinetics reported from previous time-resolved photoelectron experiments presented in the work of Kuhlman *et al.*<sup>11</sup> However, we note that Ref. 11 also reports a strong contribution from a slower time component,  $\sim 750$  fs. This is not observed within the LR-TDDFT population kinetics, but it is in very close agreement with the ADC(2) kinetics presented in the supplementary material. The exact origin for this difference between LR-TDDFT and ADC(2) is unclear; however, analysis of the *hopping* geometries indicates a flatter potential in the case of the latter, which permits a slightly wider spread of the trajectories in nuclear configuration space. Importantly, in both cases despite the small nuclear displacement required to reach the crossing point, the internal conversion from  $S_2$  to  $S_1$  is comparatively slow due to the symmetry-forbidden nature of the transition.

Once populated, the  $S_1$  undergoes a large structural distortion, primarily along the  $C_\alpha$  bond, consistent with previous work.<sup>10,18</sup> This drives the population to be rapidly transferred into the electronic ground state to form very vibrationally hot species. The fast nature of the population transfer from the  $S_1$  to the ground state means that population of the  $S_1$  does not exceed  $\sim 30\%$ . The excited state molecular dynamics consider only the dynamics within the singlet manifold. To assess the potential influence of the intersystem crossing and the triplet states, our quantum dynamics include the low-lying excited triplet states. These simulations indicate negligible amount of intersystem crossing into the triplet manifold, leading us to conclude that this channel will be unable to compete with internal conversion rates found here.

Although the excited state dynamics and high energy of excitation lead to some highly distorted geometries, our simulations point to the formation of the photoproducts being determined as the trajectory passes through the CI between the first electronically excited state and the ground state via a ring-opened intermediate. This is consistent with the conclusions from Ref. 10, whose authors demonstrated that motion away from the CI branching space leads to all of the observed photoproducts. Herein lies the most significant

approximation within our work, as neither of the single reference method used will capture the biradical nature of the photoproducts. Indeed, although all of the CIs identified<sup>18</sup> in previous work have been found within the LR-TDDFT(PBE0) framework and exist at accessible energies, i.e., below the excitation energy, our simulations show a much lower fraction of photoproduct formation than previous theoretical<sup>66,67,73,74</sup> and experimental<sup>15</sup> works. This appears to most strongly affect the C3 photoproducts, which only form in 2.5% of the trajectories. In contrast, trajectories in the T<sub>1</sub> state, performed using unrestricted Kohn–Sham facilitating the description of biradical character, initiated at random from trajectories populating the S<sub>1</sub> state, show a much higher formation of C3 photoproducts (C3: 53%, C2: 5%, and ring-open: 17%) consistent with previous experiments.<sup>15</sup> The motion through the CI and therefore the potential shape in this region is likely to be critical in determining the branching ratio of the photoproducts. Here, it may not only be a limitation of the single reference methods used but also a condition of the excited state dynamics. As stated in Sec. II C, our present dynamics attempts to avoid instabilities in the multi-configurational region, near the degeneracy by enforcing a hop to the ground state when the S<sub>1</sub>–S<sub>0</sub> energy gap became  $\Delta E_{S_1-S_0} < 0.1$  eV. While this avoids the explicit motion through the CI, the enforced earlier transition may also promote populated transfer closer the cyclobutanone structure, encouraging reformation of vibrationally hot cyclobutanone, rather than the photoproducts.

From these excited state molecular dynamics simulations, the ultrafast electron diffraction observable shows distinct changes and by studying the time-resolved PDF, these are largely associated with a loss in intensity for interactions at 1.5 and 2.5 Å, arising from dissociation. Despite the rich dynamics and the distinct changes observed, the time-resolved scattering curves show very little distinct dynamics largely associated with the incoherent nature of the dynamics and the comparatively low temporal resolution (150 fs).

Finally, a logical question would be ask if the limitations discussed above can be overcome within the present framework, i.e., without adopting a multireference wavefunction method, which would prove challenging for larger systems. Here, it is important to stress that while the relative yields of photoproducts formed appears somewhat at odds with previous works, all major reported products are generated, i.e., the full nuclear configuration space has been sampled. Excited state simulations have previously been used to simulate the experimental observables associated with structurally sensitive techniques of electron<sup>84</sup> and x-ray diffraction.<sup>35</sup> Importantly, in both of these works the outcomes of the trajectory-based dynamics were used as a basis to fit to experimental data and deliver an interpretation. Recently, forward-optimization for mapping trajectory basis functions onto time-resolved data has been shown to be highly effective.<sup>85</sup> While the use of a fit means that such an approach may not be classed as fully predictive, in both cases an excellent agreement between experiment and theory was achieved, providing deep insight into the dynamics observed.

## SUPPLEMENTARY MATERIAL

The supplementary material contains additional electronic structure calculations, expansion coefficients for the Hamiltonian, and computational details of for the quantum dynamics.

Excited state dynamics performed using ADC(2) potentials and key optimized geometries are also included.

## ACKNOWLEDGMENTS

This research made use of the Rocket High Performance Computing service at Newcastle University and the Viking High Performance Computing service at the University of York. We also acknowledge the COSMOS Program Grant (Grant No. EP/X026973/1). T.J.P would like to thank the EPSRC for an Open Fellowship (Grant No. EP/W008009/1).

## AUTHOR DECLARATIONS

### Conflict of Interest

The authors have no conflicts to disclose.

## Author Contributions

**J. Eng:** Conceptualization (equal); Data curation (equal); Formal analysis (equal); Methodology (equal); Visualization (equal); Writing – review & editing (equal). **C. D. Rankine:** Data curation (equal); Formal analysis (equal); Visualization (equal); Writing – review & editing (equal). **T. J. Penfold:** Conceptualization (equal); Data curation (equal); Formal analysis (equal); Funding acquisition (lead); Methodology (equal); Supervision (lead); Validation (equal); Visualization (equal); Writing – original draft (lead); Writing – review & editing (equal).

## DATA AVAILABILITY

The data that support the findings of this study are available from the corresponding author upon reasonable request.

## REFERENCES

- <sup>1</sup>R. Norrish and C. Bamford, “Photodecomposition of aldehydes and ketones,” *Nature* **138**, 1016 (1936).
- <sup>2</sup>N. J. Turro, J. C. Dalton, K. Dawes, G. Farrington, R. Hautala, D. Morton, M. Niemczyk, and N. Schore, “Molecular photochemistry. L. Molecular photochemistry of alkanones in solution.  $\alpha$ -cleavage, hydrogen abstraction, cycloaddition, and sensitization reactions,” *Acc. Chem. Res.* **5**, 92–101 (1972).
- <sup>3</sup>M.-H. Kao, R. K. Venkatraman, M. N. Ashfold, and A. J. Orr-Ewing, “Effects of ring-strain on the ultrafast photochemistry of cyclic ketones,” *Chem. Sci.* **11**, 1991–2000 (2020).
- <sup>4</sup>H. Denschlag and E. K. Lee, “On the mechanism of the photochemical decomposition of cyclobutanone in the gas phase,” *J. Am. Chem. Soc.* **89**, 4795–4797 (1967).
- <sup>5</sup>R. J. Campbell and E. W. Schlag, “Energy distribution in reaction products. Photolysis of cyclobutanone,” *J. Am. Chem. Soc.* **89**, 5103–5106 (1967).
- <sup>6</sup>D. R. Morton and N. J. Turro, “Photochemical ring expansion of cyclic aliphatic ketones. Cyclobutanones and cyclopentanones,” *J. Am. Chem. Soc.* **95**, 3947–3957 (1973).
- <sup>7</sup>J. C. Hemminger and E. K. Lee, “Fluorescence excitation and photodecomposition of the first excited singlet cyclobutanone (<sup>1</sup>A<sub>2</sub>): A study of predissociation of and collisional energy transfer from the vibronically selected species,” *J. Chem. Phys.* **56**, 5284–5295 (1972).

- <sup>8</sup>N. E. Lee and E. K. Lee, "Tracer study of photochemically excited cyclobutanone-2-*t* and cyclobutanone. II. Detailed mechanism, energetics, unimolecular decomposition rates, and intermolecular vibrational energy transfer," *J. Chem. Phys.* **50**, 2094–2107 (1969).
- <sup>9</sup>N. J. Turro and R. M. Southam, "Molecular photochemistry. IV. Solution photochemistry of cyclobutanone and some derivatives," *Tetrahedron Lett.* **8**, 545–551 (1967).
- <sup>10</sup>E. W.-G. Diau, C. Kötting, and A. H. Zewail, "Femtochemistry of Norrish type-I reactions: II. The anomalous predissociation dynamics of cyclobutanone on the S<sub>1</sub> surface," *ChemPhysChem* **2**, 294–309 (2001).
- <sup>11</sup>T. S. Kuhlman, T. I. Sølling, and K. B. Møller, "Coherent motion reveals non-ergodic nature of internal conversion between excited states," *ChemPhysChem* **13**, 820–827 (2012).
- <sup>12</sup>J. Zhang, W.-Y. Chiang, and J. Laane, "Jet-cooled fluorescence excitation spectra and carbonyl wagging and ring-puckering potential energy functions of cyclobutanone and its 2, 2, 4, 4-*d*<sub>4</sub> isotopomer in the S<sub>1</sub>(*n*, π\*) electronic excited state," *J. Chem. Phys.* **100**, 3455–3462 (1994).
- <sup>13</sup>E. K. Lee, J. C. Hemminger, and C. F. Rusbult, "Unusual photochemistry of cyclobutanone near its predissociation threshold," *J. Am. Chem. Soc.* **93**, 1867–1871 (1971).
- <sup>14</sup>R. F. Whitlock and A. Duncan, "Electronic spectrum of cyclobutanone," *J. Chem. Phys.* **55**, 218–224 (1971).
- <sup>15</sup>K. A. Trentelman, D. B. Moss, S. H. Kable, and P. L. Houston, "The 193-nm photodissociation of cyclobutanone: Dynamics of the C2 and C3 channels," *J. Phys. Chem.* **94**, 3031–3039 (1990).
- <sup>16</sup>M. Larsen, A. Stephansen, and T. Sølling, "Coherent motion of excited state cyclic ketones: The have and the have-nots," *Chem. Phys. Lett.* **683**, 495–499 (2017).
- <sup>17</sup>S.-H. Xia, X.-Y. Liu, Q. Fang, and G. Cui, "Excited-state ring-opening mechanism of cyclic ketones: A MS-CASPT2/CASSCF study," *J. Phys. Chem. A* **119**, 3569–3576 (2015).
- <sup>18</sup>L. Liu and W.-H. Fang, "New insights into photodissociation dynamics of cyclobutanone from the AIMS dynamic simulation," *J. Chem. Phys.* **144**, 144317 (2016).
- <sup>19</sup>A. Hopkinson, E. Lee-Ruff, and H. Lien, "Molecular orbital calculations of excited state cyclobutanone and its photocarbene," *Tetrahedron* **44**, 6815–6820 (1988).
- <sup>20</sup>F. Momicchioli, I. Baraldi, and G. Di Lonardo, "Structure of the B state of cyclobutanone," *J. Chem. Soc., Faraday Trans. 2* **71**, 791–798 (1975).
- <sup>21</sup>J. Dalton and N. Turro, "Photoreactivity of *n*, π\* excited states of alkyl ketones," *Annu. Rev. Phys. Chem.* **21**, 499–560 (1970).
- <sup>22</sup>Y. Chen and S. Ye, "Photochemical reaction mechanism of cyclobutanone: CASSCF study," *Int. J. Quantum Chem.* **97**, 725–735 (2004).
- <sup>23</sup>T. S. Kuhlman, S. Sauer, T. I. Sølling, and K. B. Møller, "Symmetry, vibrational energy redistribution and vibronic coupling: The internal conversion processes of cycloketones," *J. Chem. Phys.* **137**, 22A522 (2012).
- <sup>24</sup>T. Kuhlman, S. P. Sauer, T. I. Sølling, and K. B. Møller, "Quantum-dynamical modeling of the Rydberg to valence excited-state internal conversion in cyclobutanone and cyclopentanone," *EPJ Web Conf.* **41**, 02033 (2013).
- <sup>25</sup>G. M. Breuer and E. K. Lee, "Fluorescence decay times of cyclic ketones, acetone, and butanal in the gas phase," *J. Phys. Chem.* **75**, 989–990 (1971).
- <sup>26</sup>K. Y. Tang and E. K. Lee, "Laser photolysis of cyclobutanone. photodecomposition from selected vibronic levels at long wavelengths," *J. Phys. Chem.* **80**, 1833–1836 (1976).
- <sup>27</sup>T. S. Kuhlman, M. Pittelkow, T. I. Sølling, and K. B. Møller, "Pulling the levers of photophysics: How structure controls the rate of energy dissipation," *Angew. Chem., Int. Ed.* **52**, 2247–2250 (2013).
- <sup>28</sup>M. Ben-Nun, J. Quenneville, and T. J. Martínez, "Ab initio multiple spawning: Photochemistry from first principles quantum molecular dynamics," *J. Phys. Chem. A* **104**, 5161–5175 (2000).
- <sup>29</sup>B. F. Curchod and T. J. Martínez, "Ab initio nonadiabatic quantum molecular dynamics," *Chem. Rev.* **118**, 3305–3336 (2018).
- <sup>30</sup>D. Filippetto, P. Musumeci, R. Li, B. J. Siwick, M. Otto, M. Centurion, and J. Nunes, "Ultrafast electron diffraction: Visualizing dynamic states of matter," *Rev. Mod. Phys.* **94**, 045004 (2022).
- <sup>31</sup>C. Pellegrini, A. Marinelli, and S. Reiche, "The physics of x-ray free-electron lasers," *Rev. Mod. Phys.* **88**, 015006 (2016).
- <sup>32</sup>M. Chergui and A. H. Zewail, "Electron and X-ray methods of ultrafast structural dynamics: Advances and applications," *ChemPhysChem* **10**, 28–43 (2009).
- <sup>33</sup>J. Yang, X. Zhu, J. P. F. Nunes, J. K. Yu, R. M. Parrish, T. J. Wolf, M. Centurion, M. Gühr, R. Li, Y. Liu *et al.*, "Simultaneous observation of nuclear and electronic dynamics by ultrafast electron diffraction," *Science* **368**, 885–889 (2020).
- <sup>34</sup>T. Katayama, T.-K. Choi, D. Khakhulin, A. O. Dohn, C. J. Milne, G. Vankó, Z. Németh, F. A. Lima, J. Szlachetko, T. Sato *et al.*, "Atomic-scale observation of solvent reorganization influencing photoinduced structural dynamics in a copper complex photosensitizer," *Chem. Sci.* **14**, 2572–2584 (2023).
- <sup>35</sup>M. Minitti, J. Budarz, A. Kirrander, J. Robinson, D. Ratner, T. Lane, D. Zhu, J. Glownia, M. Kozina, H. Lemke *et al.*, "Imaging molecular motion: Femtosecond x-ray scattering of an electrocyclic chemical reaction," *Phys. Rev. Lett.* **114**, 255501 (2015).
- <sup>36</sup>TURBOMOLE V7.4.0 2019, a development of University of Karlsruhe and Forschungszentrum Karlsruhe GmbH, 1989–2007, TURBOMOLE GmbH, since 2007; available from <http://www.turbomole.com>.
- <sup>37</sup>R. Ahlrichs, M. Bär, M. Häser, H. Horn, and C. Kölmel, "Electronic structure calculations on workstation computers: The program system turbomole," *Chem. Phys. Lett.* **162**, 165–169 (1989).
- <sup>38</sup>C. Adamo and V. Barone, "Toward reliable density functional methods without adjustable parameters: The PBE0 model," *J. Chem. Phys.* **110**, 6158–6170 (1999).
- <sup>39</sup>T. H. Dunning, "Gaussian basis sets for use in correlated molecular calculations. I. The atoms boron through neon and hydrogen," *J. Chem. Phys.* **90**, 1007–1023 (1989).
- <sup>40</sup>R. A. Kendall, T. H. Dunning, and R. J. Harrison, "Electron affinities of the first-row atoms revisited. Systematic basis sets and wave functions," *J. Chem. Phys.* **96**, 6796–6806 (1992).
- <sup>41</sup>S. Hirata and M. Head-Gordon, "Time-dependent density functional theory within the Tamm–Dancoff approximation," *Chem. Phys. Lett.* **314**, 291–299 (1999).
- <sup>42</sup>C. D. Rankine, "Optci," GitLab, <https://gitlab.com/conorrankine/optci>, 2024.
- <sup>43</sup>F. Neese, "The orca program system," *WIREs Comput. Mol. Sci.* **2**, 73–78 (2011).
- <sup>44</sup>F. Neese, "Software update: The ORCA program system, version 4.0," *WIREs Comput. Mol. Sci.* **8**, e1327 (2017).
- <sup>45</sup>H. Köppel, W. Domcke, and L. S. Cederbaum, "The multi-mode vibronic coupling approach," in *Conical Intersections* (World Scientific Publishing, 2004), pp. 323–367.
- <sup>46</sup>L. S. Cederbaum, H. Köppel, and W. Domcke, "Multimode vibronic coupling effects in molecules," *Int. J. Quantum Chem.* **20**, 251–267 (2009).
- <sup>47</sup>T. J. Penfold and G. A. Worth, "A model Hamiltonian to simulate the complex photochemistry of benzene II," *J. Chem. Phys.* **131**, 064303 (2009).
- <sup>48</sup>G. Capano, T. J. Penfold, U. Röthlisberger, and I. Tavernelli, "A vibronic coupling Hamiltonian to describe the ultrafast excited state dynamics of a Cu(I)-phenanthroline complex," *Chimia* **68**, 227 (2014).
- <sup>49</sup>T. Penfold, R. Spesyvtsev, O. Kirkby, R. Minns, D. Parker, H. Fielding, and G. Worth, "Quantum dynamics study of the competing ultrafast intersystem crossing and internal conversion in the 'channel 3' region of benzene," *J. Chem. Phys.* **137**, 204310 (2012).
- <sup>50</sup>T. J. Penfold and J. Eng, "Mind the gap: Quantifying the breakdown of the linear vibronic coupling Hamiltonian," *Phys. Chem. Chem. Phys.* **25**, 7195–7204 (2023).
- <sup>51</sup>T. Pope, J. Eng, A. Monkman, and T. J. Penfold, "Spin-vibronic intersystem crossing and molecular packing effects in heavy atom free organic phosphor," *J. Chem. Theory Comput.* **20**, 1337 (2024).
- <sup>52</sup>J. Eng, Vibronic coupling maker, <https://github.com/JulienEng/VCMaker>, 2024.
- <sup>53</sup>M. H. Beck, A. Jäckle, G. A. Worth, and H.-D. Meyer, "The multiconfiguration time-dependent Hartree (MCTDH) method: A highly efficient algorithm for propagating wavepackets," *Phys. Rep.* **324**, 1–105 (2000).
- <sup>54</sup>H.-D. Meyer, F. Gatti, and G. A. Worth, *Multidimensional Quantum Dynamics: MCTDH Theory and Applications* (John Wiley & Sons, 2009).

- <sup>55</sup>G. A. Worth, K. Giri, G. W. Richings, I. Burghardt, M. H. Beck, A. Jäckle, and H.-D. Meyer, The QUANTICS Package, version 2.0, University College London London, UK, 2020.
- <sup>56</sup>M. Barbatti, M. Ruckebauer, F. Plasser, J. Pittner, G. Granucci, M. Persico, and H. Lischka, “Newton-X: A surface-hopping program for nonadiabatic molecular dynamics,” *WIREs Comput. Mol. Sci.* **4**, 26–33 (2013).
- <sup>57</sup>M. Barbatti, G. Granucci, M. Persico, M. Ruckebauer, M. Vazdar, M. Eckert-Maksić, and H. Lischka, “The on-the-fly surface-hopping program system NEWTON-X: Application to *ab initio* simulation of the nonadiabatic photo-dynamics of benchmark systems,” *J. Photochem. Photobiol., A* **190**, 228–240 (2007).
- <sup>58</sup>L. Verlet, “Computer experiments on classical fluids. I. Thermodynamical properties of Lennard-Jones molecules,” *Phys. Rev.* **159**, 98–103 (1967).
- <sup>59</sup>W. C. Swope, H. C. Andersen, P. H. Berens, and K. R. Wilson, “A computer simulation method for the calculation of equilibrium constants for the formation of physical clusters of molecules: Application to small water clusters,” *J. Chem. Phys.* **76**, 637–649 (1982).
- <sup>60</sup>S. Hammes-Schiffer and J. C. Tully, “Proton transfer in solution: Molecular dynamics with quantum transitions,” *J. Chem. Phys.* **101**, 4657–4667 (1994).
- <sup>61</sup>M. T. do Casal, J. M. Toldo, M. Pinheiro, Jr., and M. Barbatti, “Fewest switches surface hopping with Baek-An couplings,” *Open Res. Eur.* **1**, 49 (2022).
- <sup>62</sup>E. Marsili, A. Prlj, and B. F. Curchod, “Caveat when using ADC(2) for studying the photochemistry of carbonyl-containing molecules,” *Phys. Chem. Chem. Phys.* **23**, 12945–12949 (2021).
- <sup>63</sup>E. K. Lee, R. G. Shortridge, Jr., and C. F. Rusbult, “Fluorescence excitation study of cyclobutanone, cyclopentanone, and cyclohexanone in the gas phase,” *J. Am. Chem. Soc.* **93**, 1863–1867 (1971).
- <sup>64</sup>T. Penfold and G. Worth, “The effect of molecular distortions on spin-orbit coupling in simple hydrocarbons,” *Chem. Phys.* **375**, 58–66 (2010).
- <sup>65</sup>T. J. Penfold, E. Gindensperger, C. Daniel, and C. M. Marian, “Spin-vibronic mechanism for intersystem crossing,” *Chem. Rev.* **118**, 6975–7025 (2018).
- <sup>66</sup>A. M. S. Daria, J. Hernández-Rodríguez, L. M. Ibele, and S. Gómez, “Photofragmentation of cyclobutanone at 200 nm: TD-DFT vs CASSCF electron diffraction,” [arXiv:2401.07597](https://arxiv.org/abs/2401.07597) [physics.chem-ph] (2024).
- <sup>67</sup>J. Janoš, J. P. F. Nunes, D. Hollas, P. Slaviček, and B. F. E. Curchod, “Predicting the photodynamics of cyclobutanone triggered by a laser pulse at 200 nm and its MeV-UED signals—A trajectory surface-hopping and XMS-CASPT2 perspective,” [arXiv:2402.05801](https://arxiv.org/abs/2402.05801) [physics.chem-ph] (2024).
- <sup>68</sup>S. Thompson, J. Eng, and T. J. Penfold, “The intersystem crossing of a cyclic (alkyl)(amino) carbene gold (i) complex,” *J. Chem. Phys.* **149**, 014304 (2018).
- <sup>69</sup>J. Eng, S. Thompson, H. Goodwin, D. Credgington, and T. J. Penfold, “Competition between the heavy atom effect and vibronic coupling in donor-bridge-acceptor organometallics,” *Phys. Chem. Chem. Phys.* **22**, 4659–4667 (2020).
- <sup>70</sup>Q. Gu, F. Chotard, J. Eng, A.-P. M. Reponen, I. J. Vitorica-Yrezabal, A. W. Woodward, T. J. Penfold, D. Credgington, M. Bochmann, and A. S. Romanov, “Excited-state lifetime modulation by twisted and tilted molecular design in carbene-metal-amide photoemitters,” *Chem. Mater.* **34**, 7526–7542 (2022).
- <sup>71</sup>M. Baba and I. Hanazaki, “The  $S_1(n, \pi^*)$  states of cyclopentanone and cyclobutanone in a supersonic nozzle beam,” *J. Chem. Phys.* **81**, 5426–5433 (1984).
- <sup>72</sup>G. Capano, T. Penfold, M. Chergui, and I. Tavernelli, “Photophysics of a copper phenanthroline elucidated by trajectory and wavepacket-based quantum dynamics: A synergetic approach,” *Phys. Chem. Chem. Phys.* **19**, 19590–19600 (2017).
- <sup>73</sup>X. Miao, K. Diemer, and R. Mitrić, “A CASSCF/MRCI trajectory surface hopping simulation of the photochemical dynamics and the gas phase ultrafast electron diffraction patterns of cyclobutanone,” [arXiv:2401.06673](https://arxiv.org/abs/2401.06673) [physics.chem-ph] (2024).
- <sup>74</sup>J. Suchan, F. Liang, A. S. Durden, and B. G. Levine, “Prediction challenge: First principles simulation of the ultrafast electron diffraction spectrum of cyclobutanone,” [arXiv:2401.08069](https://arxiv.org/abs/2401.08069) [physics.chem-ph] (2024).
- <sup>75</sup>P. Vindel-Zandbergen and J. González-Vázquez, “Non-adiabatic dynamics of photoexcited cyclobutanone: Predicting structural measurements from trajectory surface hopping with XMS-CASPT2 simulations,” [arXiv:2402.11090](https://arxiv.org/abs/2402.11090) [physics.chem-ph] (2024).
- <sup>76</sup>D. Hait, D. Lahana, O. J. Fajen, A. S. P. Paz, P. A. Unzueta, B. Rana, L. Lu, Y. Wang, and T. J. Martinez, “Prediction of photodynamics of 200 nm excited cyclobutanone with linear response electronic structure and *ab initio* multiple spawning,” [arXiv:2402.10710](https://arxiv.org/abs/2402.10710) [physics.chem-ph] (2024).
- <sup>77</sup>J. E. Lawrence, I. M. Ansari, J. R. Mannouch, M. A. Manae, K. Asnaashari, A. Kelly, and J. O. Richardson, “A MASH simulation of the photoexcited dynamics of cyclobutanone,” [arXiv:2402.10410](https://arxiv.org/abs/2402.10410) [physics.chem-ph] (2024).
- <sup>78</sup>D. V. Makhov, A. Kirrander, and D. V. Shalashilin, “Ultrafast electron diffraction of photoexcited gas-phase cyclobutanone predicted by *ab initio* multiple cloning simulations,” [arXiv:2402.10349](https://arxiv.org/abs/2402.10349) [physics.chem-ph] (2024).
- <sup>79</sup>E. R. Miller, S. J. Hoehn, A. Kumar, D. Jiang, and S. M. Parker, “Ultrafast photochemistry and electron diffraction for cyclobutanone in the S2 state: Surface hopping with time-dependent density functional theory,” [arXiv:2402.10336](https://arxiv.org/abs/2402.10336) [physics.chem-ph] (2024).
- <sup>80</sup>L. Hutton, A. M. Carrasosa, A. W. Prentice, M. Simmermacher, J. E. Rune-son, M. J. Paterson, and A. Kirrander, “Using a multistate mapping approach to surface hopping to predict the ultrafast electron diffraction signal of gas-phase cyclobutanone,” [arXiv:2402.10195](https://arxiv.org/abs/2402.10195) [physics.chem-ph] (2024).
- <sup>81</sup>O. Bennett, A. Freibert, K. E. Spinlove, and G. A. Worth, “Prediction through quantum dynamics simulations: Photoexcited cyclobutanone,” [arXiv:2402.09933](https://arxiv.org/abs/2402.09933) [physics.chem-ph] (2024).
- <sup>82</sup>S. Mukherjee, R. S. Mattos, J. M. Toldo, H. Lischka, and M. Barbatti, “Prediction challenge: Simulating Rydberg photoexcited cyclobutanone with surface hopping dynamics based on different electronic structure methods,” [arXiv:2402.09890](https://arxiv.org/abs/2402.09890) [physics.chem-ph] (2024).
- <sup>83</sup>V. K. Jaiswal, F. Montorsi, F. Aleotti, F. Segatta, D. Keefer, S. Mukamel, A. Nenov, I. Conti, and M. Garavelli, “Ultrafast photochemistry and electron-diffraction spectra in  $n \rightarrow (3s)$  Rydberg excited cyclobutanone resolved at the multireference perturbative level,” [arXiv:2402.09873](https://arxiv.org/abs/2402.09873) [physics.chem-ph] (2024).
- <sup>84</sup>J. P. Figueira Nunes, L. M. Ibele, S. Pathak, A. R. Attar, S. Bhattacharyya, R. Boll, K. Borne, M. Centurion, B. Erk, M.-F. Lin *et al.*, “Monitoring the evolution of relative product populations at early times during a photochemical reaction,” [arXiv:2311.12482](https://arxiv.org/abs/2311.12482) (2023).
- <sup>85</sup>K. Acheson and A. Kirrander, “Robust inversion of time-resolved data via forward-optimization in a trajectory basis,” *J. Chem. Theory Comput.* **19**, 2721–2734 (2023).